# Hydrogen Bond-Mediated Self-Assembly of Polyhedral Oligomeric Silsesquioxane-Based Supramolecules

**Ruey-Sheng Shih,[†,‡] Chu-Hua Lu,[†] Shiao-Wei Kuo,*[,§] and Feng-Chih Chang*[,†]**

*Institute of Applied Chemistry, National Chiao-Tung University, 30050 Hsinchu, Taiwan, Microcell Composite Company, 717 Tainan, Taiwan, Department of Materials and Optoelectronic Science, Center for Nanoscience and Nanotechnology, National Sun Yat-Sen University, 804 Kaohsiung, Taiwan*

*Received: January 6, 2010; Revised Manuscript Received: May 30, 2010*

In this study, a functionalized pentaerythritol star polyester compound [tetrakis(nicotinoxymethyl)methane, TNMM] and an octakis[dimethyl(4-hydroxyphenethyl)siloxy]silsesquioxane (OP-POSS) were synthesized and used as tetrahedral and cubic building blocks, respectively, for three-dimensional, hydrogen-bond-mediated, polyhedral oligomeric silsesquioxane- (POSS-) based supramolecular network structures. With noncovalent chain extension of hydrogen bonds between its pyridine and phenol groups, the POSS-based supramolecular networks exhibited thermally reversible properties. Compared with the glass transition temperature of OP-POSS (ca. 20 °C) and the melting temperature of TNMM (ca. 70 °C), the hydrogen-bond-mediated miscible blend of 40 wt % TNMM in OP-POSS exhibited a single and higher glass transition temperature (37 °C). Because of its strong intermolecular hydrogen bonding, the dewetting pattern of the blend of 40 wt % TNMM in OP-POSS formed ringlike structures rather than the droplets formed by pure OP-POSS. A transparent, brittle, and glassy solid at room temperature, the blend of 40 wt % TNMM in OP-POSS is an explicit and successful example of a POSS-based hydrogen-bonded supramolecular network.

## Introduction

Hydrogen bonding is used commonly in supramolecular systems as a means of polymer formation or modification via self-assembly processes, with interaction strengths ranging widely from a few to several tens of kilojoules per mole. Central to the formation of these structures are precursor molecules of low molecular weight (usually less than 10 000), which assemble in the solid state or in solution to form aggregates of defined geometry. Intermolecular hydrogen bonds at defined positions of these building blocks, as well as their respective starting geometries and initial sizes, determine the mode of assembly into supramolecular polymers exhibiting network, rodlike, fibrous, disclike, helical, lamellar, or chainlike architectures.[1] There are two general approaches toward the preparation of such systems.[2] One is for hydrogen bonding to occur on the side chains of preformed polymers, thereby introducing new properties into the polymeric system.[3−7] Ikkala and co-workers[3,5] described a variety of side-chain polymers, with various backbones, in which phenol−pyridine hydrogen bonds between an alkylphenol species and pendent pyridyl groups led to the self-assembly of complicated and ordered microstructures. Kriz et al.[8,9] reported a related system in which the relative positions of the pyridyl and phenol units were reversed. In previous studies, we demonstrated that hydrogen bonding between pendent pyridyl and phenol groups is stronger than the dimerization of phenol itself, with a wavenumber shift of ca. 225 $cm^{-1}$.[10−13] In addition, Shibata et al.[14] investigated the thermal properties of supramolecular polymer networks formed from poly(4-vinylpyridine) and disulfonic acid, in which hydrogen bonding was used to cross-link poly(4-vinylpyridine)-based chains and, thereby, change the thermal and mechanical properties of these materials.

The second general approach toward the preparation of supramolecular polymers is for hydrogen bonding between small molecules or oligomers to be exploited for the self-assembly of extended linear chains.[15,16] Under suitable experimental conditions, such assemblies can display polymeric rheological or mechanical properties, because of their macromolecular architecture. Lehn and co-workers[17,18] used triple hydrogen-bond formation as a methodology for chain extension and for promotion of liquid crystallinity. Kim et al.[19] reported the preparation of a number of supramolecular cubes, strands, and vesicles formed through dendritic assembly. Rakotondradany et al.[20] described the chain extension of carboxy-terminated oligomers that associated through hydrogen bonding. Berl et al.[21,22] reported the self-assembly of oligopyridinecarboxamides into supramolecular strands possessing helical microstructures. Li et al.[23] used scanning tunneling microscopy to directly observe binary supramolecular assemblies comprising 1,3,5-benzenetricarboxylic acid and 4,4′-bipyridine. The use of appropriately complementary hydrogen-bond donor and acceptor structures has enabled the preparation of many interesting supramolecules exhibiting calamitic, columnar, or bent-core liquid crystalline mesophases.[24,25] In addition, some compounds of low molar mass form molecular glasses (disorderly packed solids) even in the absence of strong specific interactions between the component molecules. Nevertheless, such compounds are relatively rare and the dimensional stability of their glasses is usually low for entropy-controlled low glass transition temperatures.[26] A good way to improve the ability of low-molar-mass compounds to form glasses is to introduce hydrogen-bonding groups. For instance, mixing bisphenol A with a tetrapyridine in a 2:1 molar ratio yielded a stable glass exhibiting a glass transition at 31 °C, even though the pure components

* Corresponding authors: (F.-C.C.) tel/fax +886-3-5131512; e-mail changfc@mail.nctu.edu.tw; (S.-W.K.) fax: 886-7-5254099; e-mail: kuosw@faculty.nsysu.edu.tw.

[†] National Chiao-Tung University.

[‡] Microcell Composite Company.

[§] National Sun Yat-Sen University.

10.1021/jp1001226 
Published on Web 07/14/2010

are crystalline.[27] Low-molecular-mass glass-forming systems may find applications as hosts for blending with nonlinear optically active compounds, thereby allowing film formation while suppressing crystallization of the chromophores.[28,29]

Polyhedral oligomeric silsesquioxanes (POSSs) are well-defined molecules of nanoscale dimensions that may be functionalized with reactive groups suitable for the synthesis of new organic/inorganic hybrids, thereby providing the opportunity to build materials possessing extremely well-defined dimensions and nanophase behavior.[30−39] Consideration of their free volumes suggests that bulky POSS molecules having irregular shapes should exhibit a tendency toward the formation of glassy solids, because it would be geometrically difficult to pack POSS cubes into ordered structures without leaving large voids between cubes.[40] In previous studies,[41−45] we demonstrated that the octuply functionalized POSS products formed through hydrosilylation of octakis(dimethylsiloxy)silsesquioxane ($Q_8M_8$ POSS) with styrene or 4-acetoxysytrene are polymerlike liquids because of the presence of mixtures of isomeric $\beta$ [$R_3SiCH_2CH_2R'$] and $\alpha$ [$R_3SiCH(CH_3)R'$] linkages; we characterized these structures using $^1$H NMR spectroscopy, matrix-assisted laser desorption ionization time-of-flight (MALDI-TOF) mass spectrometry, and X-ray diffraction (XRD) analyses. In addition, octakis[dimethyl(4-hydroxyphenethyl)siloxy]silsesquioxane (OP-POSS) is a good candidate for use as a cubic "brick" for the preparation of glassy supramolecules when blended with complementary proton acceptors. Although phenol−phenol intermolecular interactions can increase the glass transition temperature of OP-POSS ($T_g$ = ca. 20 °C) relative to that of the corresponding octaphenyl congener ($T_g$ = −52 °C), OP-POSS remains a liquid because of the excessive free volume between the irregularly packed OP-POSS cubes. Although shape irregularity is an essential aspect of a material that forms a glass, rigidity and intermolecular interactions increase the value of $T_g$. Comparatively fewer studies have focused on two-component low-molecular-mass glasses.[27] We have investigated the use of tetrapyridyl, bipyridyl, and octaphenol species in place of dipyridyl−diacid,[16] dipyridyl−diphenol,[27] and dipyridiyl−triacid[46] systems as a means of counteracting the reversibility of the hydrogen bonding and, thereby, increasing the effective instantaneous chain extension in these systems.

## Experimental Section

**Materials.** Octasilane POSS was purchased from Hybrid Plastics. 4-Acetoxystyrene (96%), hydrazine monohydrate (98%), and platinum(0)−1,3-divinyl-1,1,3,3-tetramethyldisiloxane complex solution [Pt(dvs) in xylene; Pt = ca. 2%) were obtained from Aldrich Chemical. HPLC-grade solvents were used as received.

***Octakis[dimethyl(4-acetoxyphenethyl)siloxy]silsesquioxane (OA-POSS).***[41,42] 4-Acetoxystyrene (3.98 g, 23.57 mmol) was added to a solution of POSS (3.00 g, 2.95 mmol) in toluene (30 mL) in a 100-mL Schlenk flask equipped with a reflux condenser and a magnetic stirrer. The mixture was heated at 60 °C under Ar, and then Pt(dvs) (0.2 mL, 0.4 $\mu$mol) was added via syringe. The reaction was monitored in terms of the signal for the Si−H bonds at ca. 2100 cm$^{-1}$ in the Fourier transform infrared (FTIR) spectra; it was complete within 4 h. The yellowish reaction mixture was passed through neutral $Al_2O_3$ (eluent: toluene) to remove the catalyst and provide a clear, transparent solution. The solvent was evaporated under reduced pressure and the residual 4-acetoxystyrene was vacuum-distilled (ca. 0.2 Torr, 80 °C) to give OA-POSS (3.93 g, 56.3%) as a highly viscous turbid liquid that was soluble in common organic solvents [tetrahydrofuran (THF), $CHCl_3$, acetone]. $^1$H NMR (500 MHz, $CDCl_3$, ppm): $\delta$ = 6.92−7.17 (4H, aromatic C*H*), 2.62 (1.29H, $\beta$-SiCH$_2$C*H*$_2$Ar), 2.26 (1.94H, $\beta$-COOC*H*$_3$), 2.22 (1.06H, $\alpha$-COOC*H*$_3$), 1.56 [0.35H, $\alpha$-SiC*H*(CH$_3$)Ar], 1.35 [1.06H, $\alpha$-SiCH(C*H*$_3$)Ar], 0.92 (1.29H, $\beta$-SiC*H*$_2$CH$_2$Ar), −0.02 to 0.16 [6H, $\beta$- and $\alpha$-Si(C*H*$_3$)$_2$]. $^{29}$Si NMR (500 MHz, $CDCl_3$, ppm): $\delta$ = −109.3 [*Si*(O-R)$_4$], 10.2 ($\beta$-*Si*CH$_2$CH$_2$Ar), 11.9 [$\alpha$-*Si*CH(CH$_3$)Ar]. FT-IR (KBr, cm$^{-1}$): 3033 (aromatic C−H stretching), 2960 (aliphatic C−H stretching), 1765 (ester C═O stretching), 1606 (in-plane aromatic C−C stretching), 1090 (Si−O−Si stretching).

***Octakis[dimethyl(4-hydroxyphenethyl)siloxy]silsesquioxane (OP-POSS).*** Hydrazine monohydrate was added to a solution of OA-POSS (5.00 g, 2.16 mmol) in 1,4-dioxane. The hydrazinolysis of the acetyl groups was monitored in terms of the signal of the ester bonds at ca. 1740 cm$^{-1}$ in the FTIR spectra; it was complete within 2 h. The solution was added dropwise into excess deionized water and the viscous product that formed at the bottom of the beaker was collected. The product was dissolved in EtOAc and dried ($MgSO_4$); evaporation of the solvent provided a highly viscous clear liquid that was soluble in common organic solvents (THF, $CHCl_3$, and acetone). The yield of OP-POSS is 3.72 g (87%). The chemical structure and scheme for the synthesis of OP-POSS are shown in Scheme 1. $^1$H NMR (500 MHz, $CD_3OD$, ppm): $\delta$ = 6.49−7.00 (4H, aromatic C*H*), 4.51 (1H, C$_6$H$_4$O*H*), 2.52 (1.29H, $\beta$-SiCH$_2$-C*H*$_2$Ar), 2.06 [0.35H, $\alpha$-SiC*H*(CH$_3$)Ar], 1.29 [1.06H, $\alpha$-SiCH(C*H*$_3$)Ar], 0.86 (1.29H, $\beta$-SiC*H*$_2$CH$_2$Ar), −0.17−0.15 [6H, $\beta$- and $\alpha$-Si(C*H*$_3$)$_2$]. $^{29}$Si NMR (500 MHz, $CDCl_3$, ppm): $\delta$ = −109.3 [*Si*(O-R)$_4$], 10.2 ($\beta$-*Si*CH$_2$CH$_2$Ar), 11.9 [$\alpha$-*Si*CH(CH$_3$)Ar]. FT-IR (KBr, cm$^{-1}$): 3504 (free O−H), 3346 (hydrogen-bonded O−H), 3024 (aromatic C−H stretching), 2960 (aliphatic C−H stretching), 1615 (in-plane aromatic C−C stretching), 1090 (Si−O−Si stretching).

**Tetrakis(nicotinoxymethyl)methane (TNMM).**[47] A solution of nicotinic acid chloride (1.37 g, 7.70 mmol) in pyridine (30 mL) was stirred at 0 °C under an Ar atmosphere in a round-bottom two-neck 250-mL flask equipped with a magnetic stirrer, condenser, and $CaCl_2$ drying tube. A solution of pentaerythritol (0.26 g, 1.9 mmol) in pyridine (50 mL) was added to the reaction flask via a dropping funnel. After addition of triethylamine (2.14 mL, 15.4 mmol) dropwise over 1 h, the mixture was heated under reflux for 2 h. The mixture was cooled and filtered, the solvent was evaporated to dryness under reduced pressure, and then the residue was recrystallized (ethanol/water, 10:9.2 v/v) and dried under vacuum. Yield 45%. $^1$H NMR (500 MHz, $CDCl_3$, ppm): $\delta$ = 9.2 (dd, 4H, pyridyl C*H*, $J$ = 2.0, 0.7 Hz), 8.8 (dd, 4H, pyridyl C*H*, $J$ = 5.0, 1.7 Hz), 8.25 (dt, 4H, pyridyl C*H*, $J$ = 8.0, 2.0 Hz), 7.35 (ddd, 4H, pyridyl C*H*, $J$ = 8.0, 5.0, 0.7 Hz), 4.72 (s, 8H, OC*H*$_2$C). FTIR (KBr, cm$^{-1}$): 3068 (pyridyl C−H stretching), 1725 (ester C═O stretching), 1114 (ester C−O stretching).

**OP-POSS/TNMM Blends.** Mixtures of OP-POSS (10 wt %) in THF and TNMM (10 wt %) in THF/MeOH (2:1 v/v) were stirred overnight to ensure complete dissolution. The resulting solutions were mixed together at various weight ratios (Table 1) and then stirred for 6 h before being poured into a Teflon dish and heated on a hot plate at 50−60 °C for 1 day to evaporate the solvent. The blend films were then dried under vacuum to remove any residual solvent.

**Measurements.** $^1$H NMR spectra were recorded on a Varian Unity Inova 500 FT NMR spectrometer operated at 500 MHz, with $CDCl_3$ or $CD_3OD$ as the solvent; chemical shifts are reported in parts per million (ppm). For the measurement of

**SCHEME 1: Syntheses of (a) OP-POSS and (b) TNMM**

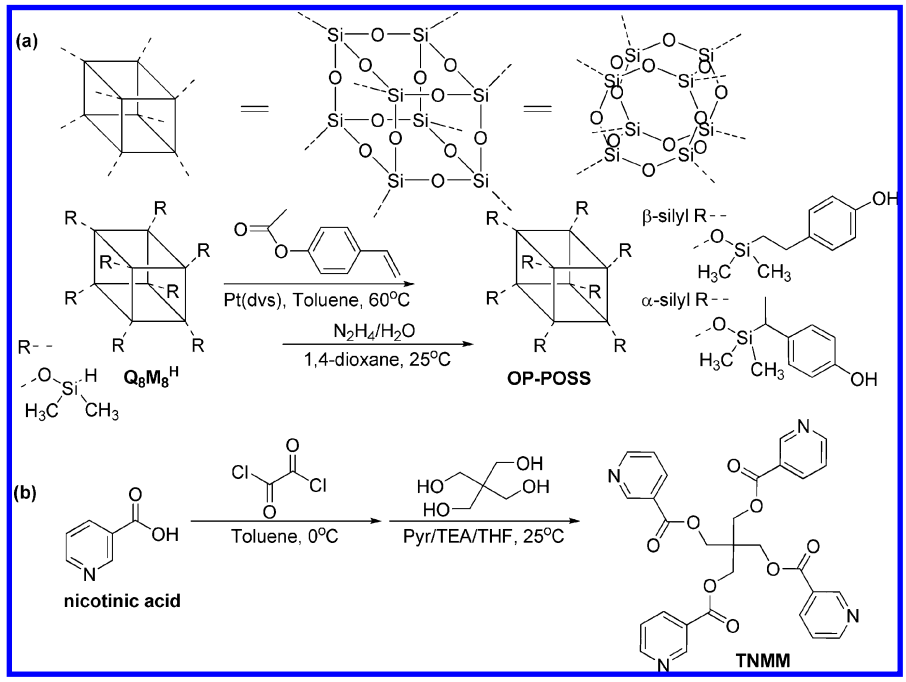


**TABLE 1: Curve-Fitting Data for the C=O Stretching Vibrations of OP-POSS/TNMM Complexes[a]**

| | free C=O | | | dipole-induced C=O | | | hydrogen-bonded C=O | | |
|---|---|---|---|---|---|---|---|---|---|
| OP-POSS/TNMM | $\nu_f$ ($cm^{-1}$) | $W_{1/2}$ ($cm^{-1}$) | $A_f$ (%) | $\nu_d$ ($cm^{-1}$) | $W_{1/2}$ ($cm^{-1}$) | $A_d$ (%) | $\nu_h$ ($cm^{-1}$) | $W_{1/2}$ ($cm^{-1}$) | $A_h$ (%) |
| 80/20 | 1737 | 13 | 36.2 | 1726 | 21 | 30.2 | 1720 | 32 | 33.6 |
| 60/40 | 1739 | 12 | 13.9 | 1727 | 19 | 54.3 | 1721 | 34 | 31.8 |
| 40/60 | 1738 | 12 | 17.1 | 1726 | 19 | 62.3 | 1718 | 36 | 20.6 |
| 20/80 | | | | 1727 | 21 | 100.0 | | | |
| 0/100 | | | | 1726 | 22 | 100.0 | | | |

[a] $\nu$ is the peak value of the assigned carbonyl group, $W_{1/2}$ is a half-height width of the Gaussian fitting band, and $A$ is an area fraction of three Gaussian bands.

a $^{29}Si$ solution NMR spectrum, any garden-variety NMR tube loaded up to a concentration of about 50−100 mg of POSS/mL of solvent run on a common 300 MHz multinuclear spectrometer with an inverse gated, 30° pulse with a 12 s delay between pulses for a couple of hours will yield a spectrum with excellent signal-to-noise. Infrared spectra were recorded on a Nicolet Avatar 320 FTIR spectrophotometer; 32 scans were collected with a spectral resolution of 1 $cm^{-1}$. Infrared spectra of polymer blend films were obtained by the conventional KBr disk method. All samples were prepared, under a continuous flow of $N_2$ to minimize sample degradation, by casting THF/MeOH solutions directly onto KBr disks and then drying under conditions similar to those used in the bulk preparation. Thermal analysis was performed on a DuPont DSC-9000 differential scanning calorimeter operated at a scan rate of 20 °C/min over a temperature range from ambient temperature to 180 °C; temperature and energy calibrations were performed with indium. A portion (ca. 5−10 mg) of each blend was weighed and sealed in an aluminum pan. This sample was rapidly cooled to −100 °C from the melt of the first scan and then rescanned from −100 to 180 °C. The glass transition temperature was obtained from the midpoint of the specific heat increment.

## Results and Discussion

**Synthesis and Characterization of OP-POSS and TNMM.** OP-POSS was prepared through the hydrosilylation of 4-acetoxystyrene with octakis(dimethylsiloxy)silsesquioxane ($Q_8M_8^H$), followed by hydrazinolysis with hydrazine monohydrate (Scheme 1a), both of which were quantitative reactions with 100% conversion. Thus, we obtained molecular mass-monodisperse OP-POSS, which we investigated using MALDI-TOF mass spectroscopy. OP-POSS was not monodisperse in terms of its structure because of the two isomeric modes of addition during hydrosilylation—that is, the $\beta$ ($R_3SiCH_2CH_2R'$) and $\alpha$ [$R_3SiCH(CH_3)R'$] linkages, where $R_3Si$ represents the POSS siloxane cage and R′ is the phenol unit. Thus, OP-POSS was a glassy liquid exhibiting a relatively low glass transition temperature (ca. 20 °C).[43] For the synthesis of TNMM, we considered the synthesis of the intermediate acid chloride from corresponding pyridinecarboxylic acid using thionyl chloride.[48,49] This procedure will lead, however, to the formation of the corresponding salt, with the chloride anion ionically bonded to the protonated pyridine ring. Applying oxalyl chloride, rather than thionyl chloride, to a suspension of the pyridinecarboxylic acid at 0 °C resulted in evaporation of HCl and formation of the nonprotonated nicotinic acid chloride,[47] which we then used in the synthesis of the corresponding pentaerythritol ester derivative (Scheme 1b). Pyridine was used in the reaction to form a reactive acetylpyridinium ion intermediate[50] and triethylamine was used to trap the formed HCl. TNMM is a crystalline powder; its melting transition, as analyzed by differential scanning calorimetry (DSC), is discussed below.

**Intermolecular Interactions of OP-POSS/TNMM Supramolecules.** The octaphenol OP-POSS formed complexes readily with the tetrapyridine TNMM to give OP-POSS/TNMM

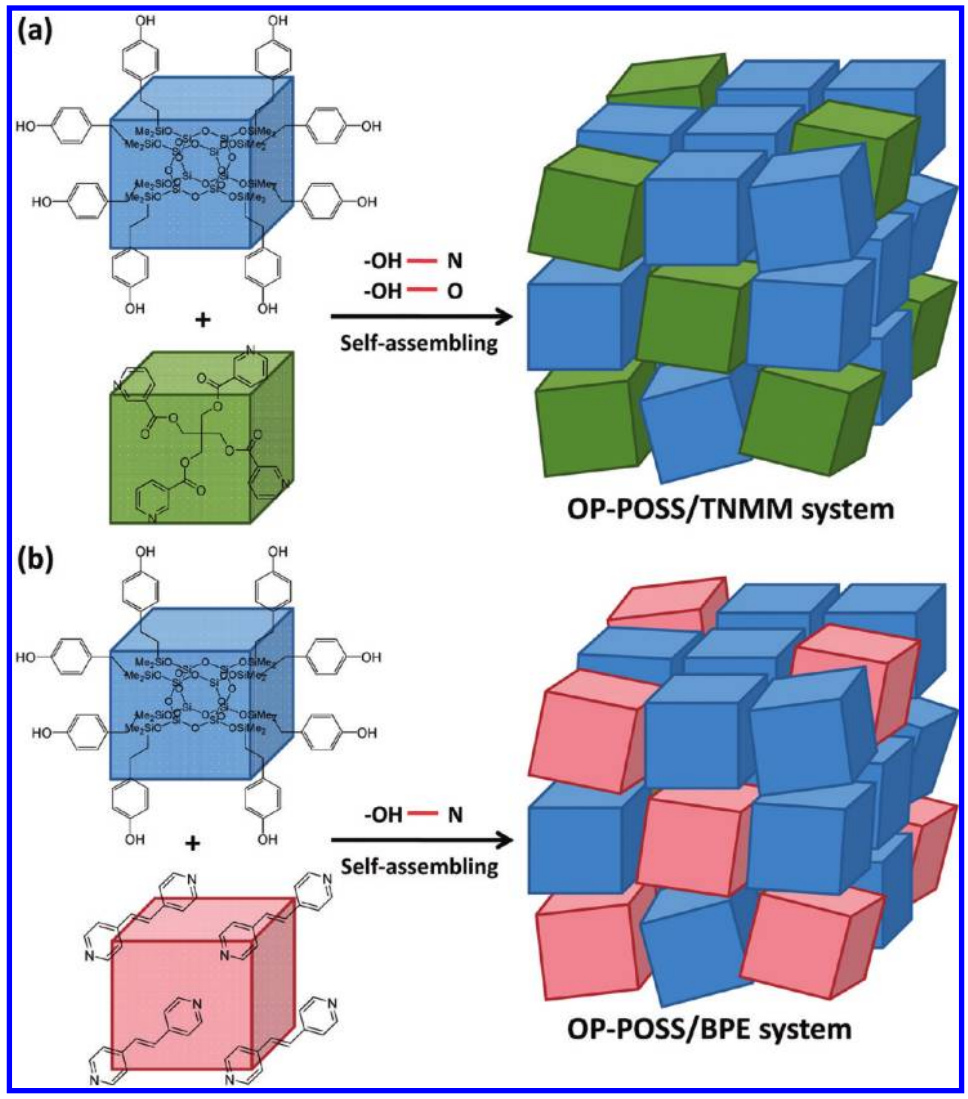


**Figure 1.** Hydrogen-bond-mediated formation of POSS-based supramolecules from (a) OP-POSS and TNMM ($A_8B_4$ polycondensation) and (b) OP-POSS and BPE ($A_8B_2$ polycondensation).

complexes incorporating various OP-POSS contents (w/w). These systems can be described as arising from reversible $A_8B_4$ polycondensation via hydrogen-bond-induced physical cross-linking (Figure 1). Confirmation of hydrogen-bond formation between the phenol and pyridine units was readily obtained by FTIR spectroscopy (Figure 2). Quantitatively, the TNMM characteristic peak of the C═O stretching modes at 1739 $cm^{-1}$ would become significant at lower OP-POSS contents, with the decreasing Si−O−Si peak assigned at 1089 $cm^{-1}$.

Figure 3 displays the hydroxyl (OH) stretching region, which was sensitive to hydrogen-bonding interactions, in the FTIR spectra of the OP-POSS/TNMM blends. Pure OP-POSS, similar to poly(vinylphenol),[10−13] displays two unresolved OH bands, one corresponding to free OH groups (at 3525 $cm^{-1}$) and the other broad band (centered at 3350 $cm^{-1}$) from the absorption of hydrogen-bonded OH groups (O−H···O−H self-association). New hydrogen-bonded OH absorption bands appeared at ca. 3165 (O−H···N) and 3450 (O−H···*O*═C) $cm^{-1}$ after hydrogen bonding occurred with the pyridyl and C═O groups. When the TNMM content in the blends reached 40 wt % (1.2 pyridine units per phenol moiety), the broad peak for phenol−phenol self-association clearly shifted to two hydrogen-bonded OH bands, reflecting that a new hydrogen-bonding distribution arosefromcompetitionbetweenO−H···O,O−H···N,andO−H···*O*═C modes.

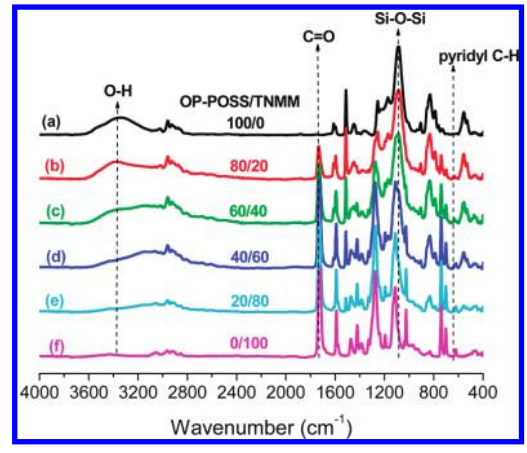


**Figure 2.** Full-range FTIR spectra (400−4000 $cm^{-1}$) of OP-POSS/TNMM blends at various weight ratios.

As expected, four types of intermolecular interactions existed to connect OP-POSS and TNMM in these hydrogen-bonded supramolecular networks (Scheme 2): phenol−phenol self-association, phenol−carbonyl hydrogen bonding, phenol−pyridine hydrogen bonding, and carbonyl−carbonyl dipole−dipole interactions. Herein, both the C═O and pyridyl groups are structural elements of TNMM. Coleman et al.[51] suggested using

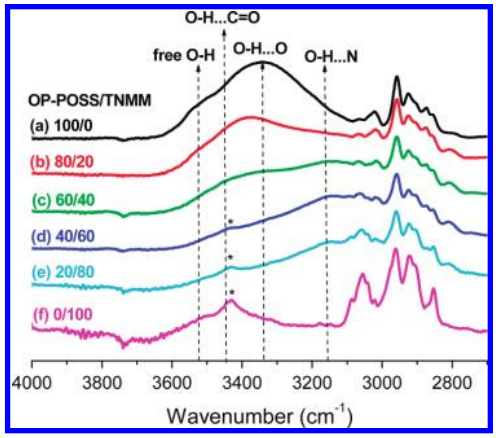


**Figure 3.** Hydroxyl region (2700−4000 $cm^{-1}$) of the FTIR spectra of OP-POSS/TNMM blends at various weight ratios. The weak peak marked with an asterisk is a C═O stretching overtone from TNMM.

**SCHEME 2: Four Types of Intermolecular Interactions in Supramolecules Composed of OP-POSS and TNMM[a]**

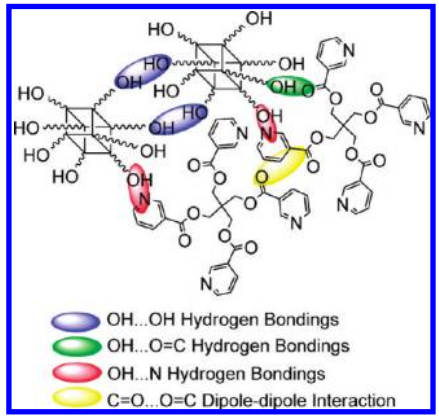


[a] (a) Phenol−phenol self-association (blue elliptic regions); (b) phenol−carbonyl hydrogen bonding (green elliptic regions); (c) phenol−pyridine hydrogen bonding (red elliptic regions); (d) carbonyl−carbonyl dipole−dipole interaction (yellow elliptic regions).

the wavenumber difference ($\Delta\nu$) between the signals of the hydrogen-bonded and free OH units to roughly estimate the average hydrogen-bonding strengths of phenol-type polymers with other proton-acceptor polymers. The hydrogen-bonding interactions between OP-POSS and TNMM can also be analyzed qualitatively and quantitatively by this method. Relative to the signal of the nonintermolecular bonding OH groups at 3525 $cm^{-1}$, we found that the intermolecular phenol-pyridine hydrogen bonds ($\Delta\nu$ = ca. 360 $cm^{-1}$) were stronger than those of both phenol−phenol self-association ($\Delta\nu$ = ca. 175 $cm^{-1}$) and phenol−carbonyl hydrogen bonding ($\Delta\nu$ = ca. 75 $cm^{-1}$). Thermodynamically, the miscibility of two components depends on the changes in enthalpy and entropy during mixing. Relative to the phenol−phenol self-association of OP-POSS molecules, the stronger phenol−pyridine hydrogen bonding reduced the mixing enthalpy, resulting in miscibility of the two components. The weaker phenol−carbonyl hydrogen bonding was, however, entropy-controlled, becoming apparent at OP-POSS/TNMM ratios greater than 40:60 (w/w).[52]

In addition to the OH stretching region, some characteristic modes of the pyridine ring are also sensitive to the existence of hydrogen bonding.[10] For example, the bands of the pyridine ring at 1590, 1050, 993, and 625 $cm^{-1}$ shifted to 1600, 1067, 1011, and 634 $cm^{-1}$, respectively, after forming hydrogen bonds with the carboxylic acid groups of poly(ethylene-*co*-methacrylic acid).[53] Unfortunately, the strongest band at 1590 $cm^{-1}$ for TNMM overlaps with that at 1600 $cm^{-1}$ for OP-POSS, resulting in an unresolved broad band. Fortunately, the band at 620 $cm^{-1}$, characteristic of the in-plane CH deformation on the pyridyl ring, can be used to analyze the strengths of the hydrogen bonds between the phenol and pyridine groups, because no significant peaks for OP-POSS appear in this region (Figure 4). Upon blending with OP-POSS, a new band appeared at 632 $cm^{-1}$, which we assigned to the hydrogen-bonded pyridyl rings. Clearly, most of the pyridine units were hydrogen-bonded to phenol moieties when the TNMM content in the blends reached 40 wt %. In addition to its effect on the wavenumber red shift, the mixture enthalpy is also an important factor affecting hydrogen-bond-mediated blending.[54−57] Poly(vinyl phenol-*co*-methyl methacrylate), for example, is a miscible copolymer because intra- or intermolecular hydrogen bonds occur preferentially between the C═O and phenol units, rather than phenol−phenol self-association.[58,59] Therefore, the dissymmetric geometries of OP-POSS and TNMM molecules could result in random packing with free pyridyl and hydrogen-bonded C═O groups (e.g., if the interaction is weaker than phenol association). As a result, we also observed signals for free pyridine units when the TNMM content was 40 wt %. Additionally, when the effect of phenol−pyridine hydrogen bonds is taken into account, the inner C═O groups of TNMM compete with both phenol and pyridine units for interaction with the phenol units, causing a blue shift of the OH band toward 3450 $cm^{-1}$ (O−H···*O*═C). The intermolecular interactions of C═O groups are, however, less readily observed than those of phenol and pyridine units. After fitting to the Gaussian function, we split the C═O stretching mode into three bands at 1738 (free), 1728 (dipole-induced, C═O···C═O), and 1718 (hydrogen-bonded, C═O···H−O) $cm^{-1}$ (Figure 5). We attribute the broad band for the hydrogen-bonded C═O groups at 1718 $cm^{-1}$ to steric effects (i.e., a wide distribution of intermolecular distances) in the phenol−pyridine hydrogen-bond-mediated supramolecular network.[60,61] We then calculated the area fraction of hydrogen-bonded C═O groups using the equation $f_b = A_b/(A_b + A_d + A_f)$, where $A_b$, $A_d$, and $A_f$ are the integral areas of the hydrogen-bonded, dipole-induced, and free C═O groups, respectively. Here, since the molar extinction coefficients of these three peaks are unknown, the area fraction of hydrogen-bonding carbonyl group is an approximation. Table 1 summarizes the results. Interestingly, hydrogen-bonded and free C═O groups coexisted, with the former reaching 33.6% in the 80 wt % OP-POSS blend. This finding indicates that the pyridine units were the preferred

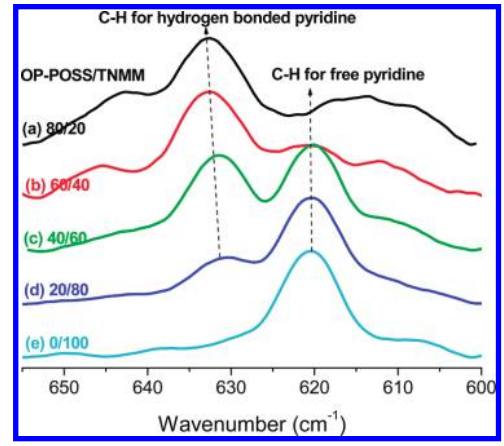


**Figure 4.** In-plane pyridyl C−H deformation region (600−655 $cm^{-1}$) of the FTIR spectra of OP-POSS/TNMM blends at various weight ratios.

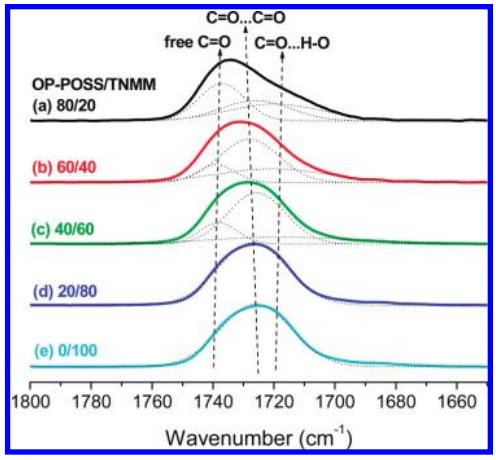


**Figure 5.** Carbonyl stretching vibration region (1650−1800 $cm^{-1}$) of the FTIR spectra of OP-POSS/TNMM blends at various weight ratios and corresponding Gaussian fitting curves.

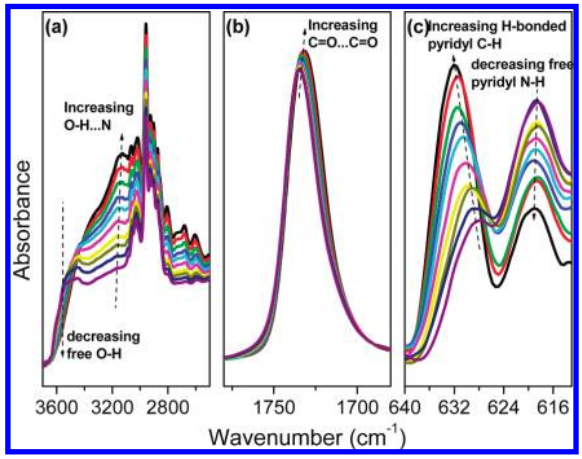


**Figure 6.** FTIR spectra displaying signals for (a) phenolic O−H, (b) C═O, and (c) pyridyl C−H vibrations for OP-POSS/TNMM blends at temperatures ranging from 210 to 30 °C (step: 20 °C).

groups forming hydrogen bonds with the phenol moieties, resulting in the high dispersion of TNMM in the hydrogen-bonded network. Thus, the inner C═O groups were isolated, appearing as free units, but the dissymmetric α- and β-hydrosilylated side chains of OP-POSS underwent phenol−carbonyl hydrogen bonding.

A temperature-dependent FTIR spectroscopic study of low-molar-mass phenol−pyridine hydrogen bonding has been reported previously.[62] In this study, we found that at 210 °C, when the blend containing 30 wt % TNMM was an isotropic liquid, absorptions appeared at 3553 and 619 $cm^{-1}$, corresponding to the free OH groups of the phenol groups of OP-POSS and the free CH groups of the pyridine units of TNMM, respectively (Figure 6). Additionally, we observed significant underlying OH absorption from OP-POSS in the range 3500−3000 $cm^{-1}$ and CH absorptions from TNMM in the range 640−624 $cm^{-1}$. Upon cooling to 30 °C, the intensities of the absorptions at 3137 and 632 $cm^{-1}$ increased (from the NH···O−H and hydrogen-bonded pyridine CH units, respectively), with concomitant reductions in the intensities of the signals of the free OH and free CH groups (3553 and 619 $cm^{-1}$, respectively); at 130 °C, the absorptions from the NH···O−H and the hydrogen-bonded pyridine CH units become even more intense. Thus, the extent of hydrogen bonding between the phenol and pyridine units increased upon cooling from the isotropic liquid to the solid state. Hydrogen bonding did occur in the isotropic liquid, but

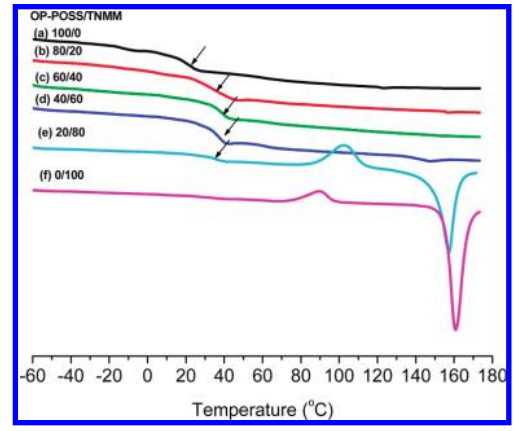


**Figure 7.** Second-heating DSC thermograms of OP-POSS/TNMM blends at various weight ratios.

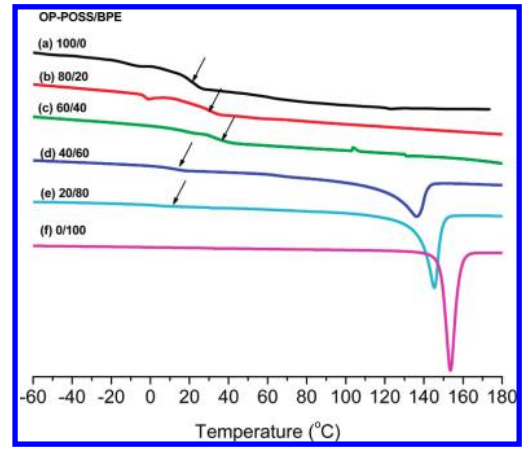


**Figure 8.** Second-heating DSC thermograms of OP-POSS/BPE blends at various weight ratios.

the dynamics of hydrogen-bond formation and dissociation were sufficiently rapid that a significant number of OH and CH groups were free (not subject to intermolecular interactions) at any instant.[63] When the temperature decreases, it is likely that the dynamics of the association and dissociation processes will be slowed. Thus, the octafunctionalized OP-POSS and the tetrafunctionalized TNMM formed an $A_8B_4$ network possessing a reversibly branched structure.

**Thermal Properties of OP-POSS/TNMM Complexes.** DSC analyses of OP-POSS/TNMM (Figure 7) and OP-POSS/BPE (Figure 8) blends provided further insight into the behavior of the hydrogen-bonding supramolecules. The DSC trace of pure OP-POSS revealed that, upon heating, the onset of the glass transition occurred at a temperature of ca. 20 °C, suggesting that pure OP-POSS was a viscous fluid at 25 °C. The DSC trace of pure TNMM (Figure 7f) reveals that, upon heating, the onsets of the recrystallization exotherm and melting endotherm occurred at 70.6 and 146.6 °C, respectively. In contrast, the DSC trace of pure BPE (Figure 8f) reveals only one melting endotherm, with an onset temperature of 136.3 °C. The presence of a recrystallization exotherm in Figure 7f suggests that the bulky TNMM molecules required more time to pack into their crystal structure than did the linear BPE molecules into theirs (Figure 8f). Thus, upon heating of the rapidly cooled TNMM, recrystallization occurred to reconstruct its crystals.

The glass transition temperature is an important physical property reflecting a change in intermolecular interactions; it is readily measured by DSC. Table 2 lists the glass transition temperatures ($T_g$) and transition ranges ($\Delta T_g$) for blends of OP-

**TABLE 2: Glass Transition Temperatures and Transition Temperature Ranges of Various OP-POSS/TNMM Blends**

| blending ratio (wt %) | $T_g$ (°C) | $\Delta T_g$ (°C) |
|---|---|---|
| 100/0 | 14.4 | 23.7 |
| 80/20 | 34.0 | 19.5 |
| 60/40 | 36.2 | 12.4 |
| 40/60 | 34.7 | 11.2 |
| 20/80 | 35.1 | 7.4 |
| 0/100 | 28.0 | 20.0 |

POSS and TNMM. In addition to the crystal region of TNMM, its single glass transition temperature strongly suggests that the amorphous domain is miscible at dimensions of less than 20−40 nm. When the OP-POSS/TNMM ratio is increased to 40:60, the crystal domains of TNMM were destroyed through the C═O dipole−dipole interactions being replaced by strong phenol−pyridine or weak phenol−carbonyl hydrogen bonds. This behavior is evidenced by the fact that, at a OP-POSS/TNMM ratio of 80:20 (w/w), the value of $T_g$ increased by 20 °C relative to that of pure OP-POSS. On the basis of the results of our FTIR spectroscopic and DSC analyses, we chose an OP-POSS/TNMM ratio of 70:30 as being optimal for the preparation of polymeric membrane films; Figure 9 displays images of two such pieces of transparent supramolecular films. At this composition, TNMM interacted with OP-POSS through phenol−pyridine hydrogen bonds; TNMM did not form weak phenol−carbonyl hydrogen bonds or feature its crystal domain. Although we did improve the glass transition temperature of OP-POSS in this study, its supramolecular films were brittle at room temperature and broke into several pieces under an external force load. Nevertheless, this study suggested to us that in the future we should prepare more practical supramolecules incorporating more covalent bonding sites and more flexible oligomer chains.

**Transmission Electron Microscopy of Aggregate Structures.** In addition to FTIR spectroscopic studies and thermal analyses, we also used transmission electron microscopy (TEM) to observe the aggregate structures, on the (sub)micrometer scale, formed after solution-casting a mixture of OP-POSS and TNMM. Figure 10a,b reveals that pure OP-POSS aggregated into separate spherical drops (average diameter 0.45 $\mu$m), whereas the 60:40 blend of OP-POSS/TNMM formed uniform ringlike structures (average inner spherical diameter 9.14 $\mu$m; average ring thickness 0.76 $\mu$m). Pointed arrayed structures of aggregated pure OP-POSS, with an average center-to-center distance of 2 $\mu$m, are usually formed through dewetting processes during solvent evaporation.[64] Micrometer-sized ring structures can arise as a result of the evaporation-driven instability of hole nucleation.[65,66] Figure 10c displays the ring-spot complex structure of the aggregate formed from the 80:20 OP-POSS/TNMM blend. When the ratio of OP-POSS/TNMM was increased to more than 60:40, the aggregate structure transformed into spherical drops having sizes ranging from 0.5 to 2 $\mu$m. Because these TEM samples were prepared under the same conditions (concentration, temperature, and time), we conclude that the OP-POSS/TNMM composition ratio played the dominant role during the formation of the distinct microsized aggregates. Because the strength of intermolecular interactions depended on the OP-POSS/TNMM blending ratio, we suspect that replacing phenol−phenol self-association with phenol−pyridine and/or phenol−carbonyl hydrogen bonds caused the change in the aggregation microstructures from submicrometer spots to micrometer rings. Figure 11 displays the possible mechanisms for the formation of separate spherical drops from pure OP-POSS and uniform ringlike structures from the OP-POSS/TNMM complex.

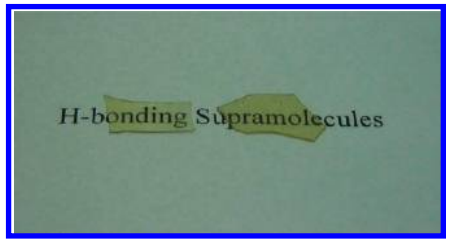


**Figure 9.** Two pieces of transparent supramolecular films prepared at an OP-POSS/TNMM blending ratio of 70:30.

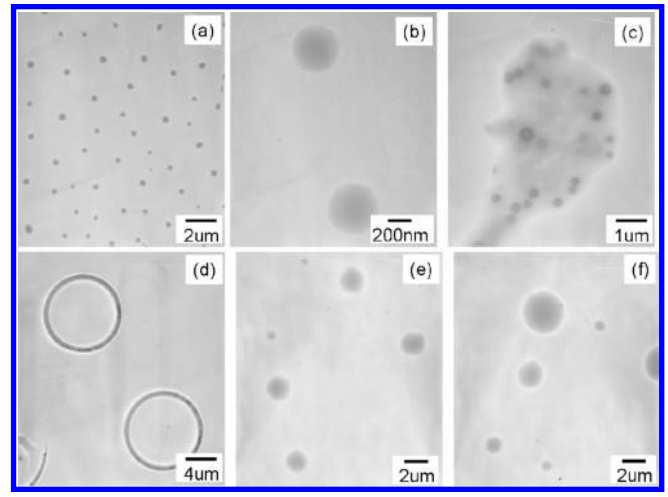


**Figure 10.** TEM micrographs of aggregate structures formed from OP-POSS/TNMM mixtures at blend ratios of (a) 100:0 (low magnitude), (b) 100:0 (high magnitude), (c) 80:20, (d) 60:40, (e) 40:60, and (f) 20:80.

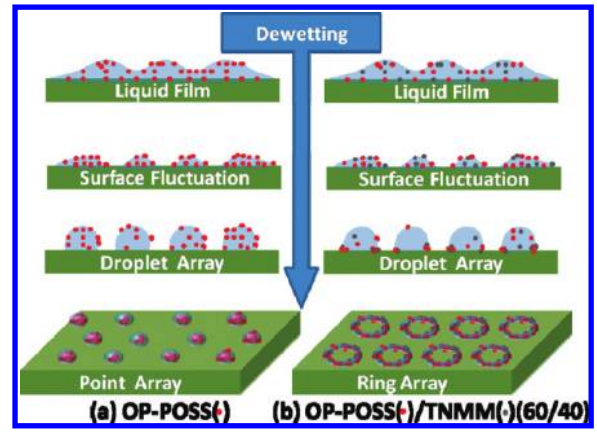


**Figure 11.** Proposed mechanisms for the formation of separate spherical drops of pure OP-POSS and uniform ringlike structures of OP-POSS/TNMM complexes.

## Conclusion

We have prepared new supramolecular structures from the interactions between a POSS derivative and TNMM. FTIR spectroscopy provided clear evidence for the formation of intermolecular hydrogen bonds between the OP-POSS and TNMM units. In addition, DSC thermograms revealed that a TNMM content of 40 wt % provided the strongest intermolecular interactions, with the glass transition temperatures being an indication of degree of local intermolecular thermal motion. This blend ratio allowed the preparation of hydrogen-bond-induced glassy rings ($T_g$ = 36.2 °C), which may be of practical interest for the fabrication of ordered patterns without using

lithography; for example, such 10-$\mu$m rings on a wafer might be useful as a barrier for biocells for further morphological or electrical analyses. During the dewetting process, the liquid thin film formed a point array of solution droplets as a result of surface concentration fluctuation. Even though high concentration appeared at the three-phase interface of the droplets during rapid solvent evaporation, the dispersion of solutes was driven thermodynamically by entropy effects. Pure OP-POSS formed a point array on the carbon-coated copper grid; when blended with 40 wt % TNMM, however, strong phenol−pyridine hydrogen bonding between the OP-POSS and TNMM units induced insoluble aggregates to form at the three-phase interface, subsequently undergoing heterogeneous solidification to give microsized ring structures.

**Acknowledgment.** This work was supported financially by the National Science Council of the ROC under Contracts NSC 97-2221-E-110-013-MY3 and NSC 98-2221-E-110-006.

## References and Notes

(1) Binder, W.; Zirbs, R. *Adv. Polym. Sci.* **2007**, *207*, 1.
(2) Pourcain, C.; Griffin, A. C. *Macromolecules* **1995**, *28*, 4116.
(3) Ruokolainen, J.; Saariaho, M.; Ikkala, O.; ten Brinke, G.; Thomas, E. L.; Torkkeli, M.; Serimaa, R. *Macromolecules* **1999**, *32*, 1152.
(4) Wu, X.; Zhang, G.; Zhang, H. *Macromol. Chem. Phys.* **1998**, *199*, 2101.
(5) Ruokolainen, J.; Torkkeli, M.; Serimaa, R.; Komanschek, E.; ten Brinke, G.; Ikkala, O. *Macromolecules* **1997**, *30*, 2002.
(6) Sheen, Y. C.; Lu, C. H.; Huang, C. F.; Kuo, S. W.; Chang, F. C. *Polymer* **2008**, *49*, 4017.
(7) Vera, F.; Almuzara, C.; Orera, I.; Barbera, J.; Oriol, L.; Serrano, J. L.; Sierra, T. *J. Polym. Sci., Part A: Polym. Chem.* **2008**, *46*, 5528.
(8) Kriz, J.; Dybal, J. *J. Phys. Chem. B* **2005**, *109*, 13436.
(9) Kriz, J.; Dybal, J.; Brus, J. *J. Phys. Chem. B* **2006**, *110*, 18338.
(10) Kuo, S. W.; Lin, C. L.; Chang, F. C. *Polymer* **2002**, *43*, 3943.
(11) Kuo, S. W.; Tung, P. H.; Chang, F. C. *Macromolecules* **2006**, *39*, 9388.
(12) Kuo, S. W.; Tung, P. H.; Lai, C. L.; Jeong, K. U.; Chang, F. C. *Macromol. Rapid Commun.* **2008**, *29*, 229.
(13) Kuo, S. W.; Tung, P. H.; Chang, F. C. *Eur. Polym. J.* **2009**, *45*, 1924.
(14) Shibata, M.; Kimura, Y.; Yaginuma, D. *Polymer* **2004**, *45*, 7571.
(15) Bladon, P.; Griffin, A. C. *Macromolecules* **1993**, *26*, 6604.
(16) Bouteiller, L. *Adv. Polym. Sci.* **2007**, *27*, 79.
(17) Fouquey, C.; Lehn, J. M.; Levelut, A. M. *Adv. Mater.* **1990**, *2*, 254.
(18) Lehn, J. M.; Mascal, M.; DeCian, A.; Fischer, J. *J. Chem. Soc., Perkin Trans.* **1992**, *2*, 461.
(19) Kim, C.; Lee, S. J.; Lee, I. H.; Kim, K. T. *Chem. Mater.* **2003**, *15*, 3638.
(20) Rakotondradany, F.; Whitehead, M. A.; Lebuis, A. M.; Sleiman, H. F. *Chem.—Eur. J.* **2003**, *9*, 4771.
(21) Berl, V.; Huc, I.; Khoury, R. G.; Krische, M. J.; Lehn, J. M. *Nature* **2000**, *407*, 720.
(22) Berl, V.; Schmutz, M.; Krische, M. J.; Khoury, R. G.; Lehn, J. M. *Chem.—Eur. J.* **2002**, *8*, 1227.
(23) Li, M.; Yang, Y. L.; Zhao, K. Q.; Zeng, Q. D.; Wang, C. *J. Phys. Chem. C* **2008**, *112*, 10141.
(24) Beginn, U. *Prog. Polym. Sci.* **2003**, *28*, 1049.
(25) Kato, T.; Mizoshita, N.; Kishimmoto, K. *Angew. Chem., Int. Ed.* **2006**, *45*, 38.
(26) Alig, I.; Braun, D.; Langendorf, R.; Wirth, H. O.; Voigt, M.; Wendorff, J. H. *J. Mater. Chem.* **1998**, *8*, 847.
(27) Boileau, S.; Bouteiller, L.; Foucat, E.; Lacoudre, N. *J. Mater. Chem.* **2002**, *12*, 195.
(28) Smets, G. *Adv. Polym. Sci.* **1983**, *50*, 17.
(29) Osakeni, J. A.; Jenekhe, S. A. *Macromolecules* **1994**, *27*, 739.
(30) Pielichowski, K.; Njuguna, J.; Janowski, B.; Pielichowski, J. *Adv. Polym. Sci.* **2006**, *201*, 225.
(31) Xu, H.; Kuo, S. W.; Lee, J. S.; Chang, F. C. *Macromolecules* **2002**, *35*, 8788.
(32) Xu, H.; Kuo, S. W.; Lee, J. S.; Chang, F. C. *Polymer* **2002**, *43*, 5117.
(33) Lee, Y. J.; Kuo, S. W.; Huang, W. J.; Lee, H. Y.; Chang, F. C. *J. Polym. Sci.: Polym. Phys.* **2004**, *42*, 1127.
(34) Wu, J.; Haddad, T. S.; Mather, P. T. *Macromolecules* **2009**, *42*, 1142.
(35) Huang, C. F.; Kuo, S. W.; Lin, F. J.; Huang, W. J.; Wang, C. F.; Chen, W. Y.; Chang, F. C. *Macromolecules* **2006**, *39*, 300.
(36) Lee, Y. J.; Kuo, S. W.; Huang, C. F.; Chang, F. C. *Polymer* **2006**, *47*, 4378.
(37) Lu, C. H.; Kuo, S. W.; Huang, C. F.; Chang, F. C. *J. Phys. Chem. C* **2009**, *113*, 3517.
(38) Kuo, S. W.; Lee, H. F.; Huang, W. J.; Jeong, K. U.; Chang, F. C. *Macromolecules* **2009**, *42*, 1619.
(39) Kuo, S. W.; Wu, Y. C.; Lu, C. H.; Chang, F. C. *J. Polym. Sci.: Polym. Phys.* **2009**, *47*, 811.
(40) Bueche, F. *Physical Properties of Polymers*; Interscience Publishers: New York, 1962, p 85.
(41) Kuo, S. W.; Lin, H. C.; Huang, W. J.; Huang, C. F.; Chang, F. C. *J. Polym. Sci.: Polym. Phys.* **2006**, *44*, 673.
(42) Lin, H. C.; Kuo, S. W.; Huang, C. F.; Chang, F. C. *Macromol. Rapid Commun.* **2006**, *27*, 537.
(43) Yen, Y. J.; Kuo, S. W.; Huang, C. F.; Chen, J. K.; Chang, F. C. *J. Phys. Chem. B* **2008**, *112*, 10821.
(44) Huang, K. W.; Tsai, L. W.; Kuo, S. W. *Polymer* **2009**, *50*, 4876.
(45) Lu, C. H.; Kuo, S. W.; Chang, W. T.; Chang, F. C. *Macromol. Rapid Commun.* **2009**, *30*, 2121.
(46) Kihara, H.; Kato, T.; Uryu, T.; Frechet, J. M. J. *Chem. Mater.* **1996**, *8*, 961.
(47) Kalle, I. N.; Rissanen, K. *Cryst. Growth Des.* **2003**, *3*, 339.
(48) Riberau, P.; Queguiner, G. *Can. J. Chem.* **1983**, *61*, 334.
(49) Park, Y. T.; Jung, C. H.; Kim, K. W. *J. Org. Chem.* **1999**, *64*, 8546.
(50) Fersht, A. R.; Jencks, W. P. *J. Am. Chem. Soc.* **1970**, *92*, 5432.
(51) Coleman, M. M.; Graf, J. F.; Painter, P. C. *Specific Interaction and the Miscibility of Polymer Blends*; Technomic Publishing Co.: Lancaster, PA, 1991.
(52) Kuo, S. W.; Chan, S. C.; Wu, H. D.; Chang, F. C. *Macromolecules* **2005**, *38*, 4729.
(53) Lee, Y. J.; Painter, P. C.; Coleman, M. M. *Macromolecules* **1988**, *21*, 954.
(54) Painter, P. C.; Veytsman, B.; Kumar, S.; Shenoy, S.; Graf, J. F.; Xu, Y.; Coleman, M. M. *Macromolecules* **1997**, *30*, 932.
(55) Coleman, M. M.; Pehlert, G. J.; Painter, P. C. *Macromolecules* **1996**, *29*, 6820.
(56) Pehlert, G. J.; Painter, P. C.; Veytsman, B.; Coleman, M. M. *Macromolecules* **1997**, *30*, 3671.
(57) Pehlert, G. J.; Painter, P. C.; Coleman, M. M. *Macromolecules* **1998**, *31*, 8423.
(58) Lin, C. L.; Chen, W. C.; Liao, C. S.; Su, Y. C.; Huang, C. F.; Kuo, S. W.; Chang, F. C. *Macromolecules* **2005**, *38*, 6435.
(59) Lin, C. L.; Chen, W. C.; Kuo, S. W.; Chang, F. C. *Polymer* **2006**, *47*, 3436.
(60) Ishida, H.; Lee, Y. H. *J. Polym. Sci., Part B: Polym. Phys.* **2001**, *39*, 73.
(61) Ishida, H.; Lee, Y. H. *J. Appl. Polym. Sci.* **2001**, *81*, 1021.
(62) Kato, T.; Uryu, T.; Kaneuchi, F.; Jin, C.; Frechet, J. M. J. *Liq. Cryst.* **1993**, *14*, 1311.
(63) Lee, C. M.; Jariwaia, C. P.; Griffin, A. C. *Polymer* **1994**, *35*, 4550.
(64) Suematsu, N. J.; Ogawa, Y.; Yamamoto, Y.; Yamaguchi, T. *J. Colloid Interface Sci.* **2007**, *310*, 648.
(65) Tripp, S. L.; Pusztay, S. V.; Ribbe, A. E.; Wei, A. *J. Am. Chem. Soc.* **2002**, *124*, 7914.
(66) Ohara, P. C.; Gelbart, W. M. *Langmuir* **1998**, *14*, 3418.

JP1001226